

Comparative linkage mapping uncovers massive chromosomal inversions associated with local adaptation in Atlantic silversides

Maria Akopyan*, Anna Tigano^{†,1}, Arne Jacobs^{†,2}, Aryn P. Wilder^{†,3}, Hannes Baumann[‡], Nina O. Therkildsen[†]

* Department of Ecology and Evolutionary Biology, Cornell University, NY, USA

† Department of Natural Resources and the Environment, Cornell University, NY, USA

‡ Department of Marine Sciences, University of Connecticut, CT, USA

¹ Department of Biology, UBC Okanagan Campus, British Columbia, Canada

² Institute of Biodiversity Animal Health & Comparative Medicine, University of Glasgow, UK

³ Conservation Science Wildlife Health, San Diego Zoo Wildlife Alliance, CA, USA

Keywords: linkage map, recombination, inversion, local adaptation, heterochiasmy, Atlantic silverside

Running title: Chromosomal inversions in Atlantic silversides

Corresponding author: Maria Akopyan, ma2256@cornell.edu

1 Abstract

2

3 The role of recombination in genome evolution has long been studied in theory, but until recently
4 empirical investigations had been limited to a small number of model species. Here we compare the
5 recombination landscape and genome collinearity between two populations of the Atlantic silverside
6 (*Menidia menidia*), a small fish distributed across the steep latitudinal climate gradient of the North
7 American Atlantic coast. Using ddRADseq, we constructed separate linkage maps for locally adapted
8 populations from New York and Georgia and their inter-population lab cross. First, we used one of the
9 linkage maps to improve the current silverside genome assembly by anchoring three large unplaced
10 scaffolds to two chromosomes. Second, we estimated sex-specific recombination rates, finding 2.3-fold
11 higher recombination rates in females than males—one of the most extreme examples of
12 heterochiasmy in a fish. While recombination occurs relatively evenly across female chromosomes, it
13 is restricted to only the terminal ends of male chromosomes. Furthermore, comparisons of female
14 linkage maps revealed suppressed recombination along several massive chromosomal inversions
15 spanning nearly 16% of the genome that segregate between locally adapted populations and coincide
16 near perfectly with blocks of highly elevated genomic differentiation between wild populations.
17 Finally, we discerned significantly higher recombination rates across chromosomes in the northern
18 population. In addition to providing valuable resources for ongoing evolutionary and comparative
19 genomic studies, our findings represent a striking example of structural variation that impacts
20 recombination between adaptively divergent populations, providing empirical support for theorized
21 genomic mechanisms facilitating adaptation despite gene flow.

22

23

24 Introduction

25

26 Recombination is a fundamental evolutionary mechanism that influences genetic variation and
27 adaptive trajectories. The exchange of alleles onto different genetic backgrounds as a result of
28 recombination can both facilitate and impede adaptive evolution (Tigano and Friesen 2016). It can
29 promote adaptation by generating novel combinations of beneficial haplotypes (Felsenstein 1974), or
30 by breaking up genetic associations to allow the purging of deleterious mutations from adaptive

31 haplotypes (Muller 1964). Conversely, recombination can disrupt favorable allelic combinations, which
32 in turn can reduce the fitness of a population (Smith 1978; Altenberg and Feldman 1987).
33 Understanding the role of recombination in facilitating responses to selection has been the subject of
34 extensive theoretical study (Felsenstein 1974; Otto and Barton 1997; Barton and Charlesworth 1998;
35 Otto and Lenormand 2002), and a growing body of empirical evidence has demonstrated that
36 recombination varies highly among taxa and can contribute to different patterns of genetic diversity
37 and divergence across species (Dapper and Payseur 2017; Ritz *et al.* 2017; Stapley *et al.* 2017). This
38 supports the notion that recombination plays a crucial role in genome evolution.

39
40 Studies in a wide range of species have shown that recombination also tends to vary across the genome
41 both within and among chromosomes (Begun and Aquadro 1992; Wu *et al.* 2003; Anderson *et al.* 2006;
42 Kim *et al.* 2007; Branca *et al.* 2011; Hinch *et al.* 2011; Haenel *et al.* 2018). In most cases, recombination
43 is reduced at the center of chromosomes, with the rate of crossovers gradually increasing towards the
44 telomeres. This variation in recombination along the genome – the recombination landscape – has a
45 profound impact on the efficacy of selection. Genomic features that can alter recombination rates and
46 maintain linkage between adapted alleles in the presence of gene flow may be favored by selection
47 (Noor *et al.* 2001; Rieseberg 2001; Nosil *et al.* 2009). Structural rearrangements including inversions,
48 translocations, and fusions, can thus have a considerable effect on genetic transmission by interfering
49 with recombination and promoting genome divergence (Tigano and Friesen 2016; Wellenreuther and
50 Bernatchez 2018).

51
52 Among structural variants, chromosomal inversions are known to strongly shape local recombination
53 landscapes (Stevison *et al.* 2017). The key evolutionary effect of inversions is that they suppress
54 recombination in a heterozygous state (Sturtevant and Beadle 1936). By suppressing recombination in
55 heterokaryotypes, inverted chromosomal regions can capture multiple loci involved in adaptation to
56 contrasting environments and protect these favorable combinations of adaptive alleles (Kirkpatrick and
57 Barton 2006; Hoffmann and Rieseberg 2008; Yeaman 2013). Recombination continues normally in the
58 homozygous state for inverted and uninverted haplotypes, respectively, allowing inversions to escape
59 some of the deleterious consequences suffered when recombination is entirely suppressed (Kirkpatrick
60 2010). While inversion polymorphisms capturing locally adapted loci are predicted to be a favorable

61 architecture for adaptation despite gene flow (Kirkpatrick and Barton 2006; Yeaman 2013), until
62 recently, much of the evidence supporting the role of inversions in adaptation came from a few classic
63 examples (Krimbas and Powell 1992; Stefansson *et al.* 2005; Joron *et al.* 2006).

64

65 Increasing accessibility to genomic sequence data has led to the discovery that structural genomic
66 variants are associated with adaptive divergence in a wide range of species (Wellenreuther *et al.* 2019;
67 Mérot 2020). For instance, inversions maintain genomic differentiation between migratory and
68 stationary ecotypes of the Atlantic cod (*Gadhus morhua*; Kirubakaran *et al.* 2016; Sodeland *et al.* 2016).
69 In the seaweed fly (*Coelopa frigida*), alternate haplotypes have opposing effects on larval survival and
70 adult reproduction (Mérot *et al.* 2020). Clinal patterns of polymorphic inversions also underlie locally
71 adapted ecotypes of a coastal marine snail (*Littorina saxatilis*; Faria *et al.* 2019a) and have played an
72 important role in repeated evolution of marine and freshwater sticklebacks (*Gasterosteus aculeatus*;
73 Jones *et al.* 2012; Roesti *et al.* 2015). While many examples of inversions associated with local
74 adaptations come from aquatic systems where there is typically high gene flow counteracting adaptive
75 divergence among populations, there is also evidence of chromosomal rearrangements facilitating
76 adaptation to terrestrial environments (e.g., Christmas *et al.* 2019; Todesco *et al.* 2020; Hager *et al.*
77 2021). Despite a growing appreciation for the effects of recombination on the dynamics of selection,
78 the genomic features affecting the recombination landscape are still poorly understood in many
79 systems because most studies have historically been limited to inbred lines of cultivated or model
80 species (Stapley *et al.* 2017). Even less is known about the variation in recombination rates and genome
81 structure across diverging populations of the same species (Samuk *et al.* 2020; Schwarzkopf *et al.* 2020),
82 especially in an ecological context—i.e., non-model natural populations examined across varying
83 environments (Stapley *et al.* 2017).

84

85 Distributed across the world's steepest latitudinal climate gradient along North America's Atlantic
86 coast (Baumann and Doherty 2013), Atlantic silversides (*Menidia menidia*, hereafter: silversides)
87 exhibit a remarkable degree of local adaptation in a suite of physiological and morphological traits
88 (Conover *et al.* 2005). For example, the species exhibits countergradient variation in growth capacity
89 (Conover and Present 1990), whereby northernmost populations have evolved higher growth capacity
90 in response to shorter growing seasons, whereas tradeoffs with predator avoidance have selected for

91 slower growth in the south (Billerbeck *et al.* 2001; Munch and Conover 2003; Arnott *et al.* 2006).
92 Silverside populations also exhibit clinal genetic variation in vertebral number, temperature-dependent
93 sex determination, swimming performance, lipid storage, spawning temperature and duration, egg
94 volume, egg production, and size of offspring at hatch (Conover *et al.* 2009). Due to their broad
95 distribution, abundance, and relative ease of husbandry, Atlantic silversides have been the focus of a
96 wide range of ecological and evolutionary studies, such as experiments on fisheries-induced evolution
97 (Conover and Munch 2002), responses to climate change (DePasquale *et al.* 2015; Murray *et al.* 2016),
98 and local adaptation (Conover and Heins 1987; Conover and Present 1990; Schultz *et al.* 1998).
99 However, after decades of research, we are only just beginning to explore the genomic basis underlying
100 the remarkable capacity for adaptation in this ecological and evolutionary model species (Therkildsen
101 *et al.* 2019; Therkildsen and Baumann 2020; Wilder *et al.* 2020; Tigano *et al.* 2021a).

102
103 Our recent work started to examine the genomic basis of local adaptation in Atlantic silversides,
104 revealing variation in genome structure among populations. We discovered that despite high gene flow
105 maintaining overall low levels of genome divergence between populations, large blocks of the genome
106 show strong linkage disequilibrium (LD) and differentiation between populations (Wilder *et al.* 2020;
107 Tigano *et al.* 2021a). Strong LD spanning millions of bases, including thousands of variants fixed for
108 alternate alleles in different populations, supported the presence of chromosomal inversions that
109 maintain divergent adaptive haplotypes between highly connected silverside populations (Therkildsen
110 *et al.* 2019; Therkildsen and Baumann 2020; Wilder *et al.* 2020; Tigano *et al.* 2021a). Subsequent
111 alignments of genome assemblies from northern and southern populations and comparative analysis of
112 the linear order of scaffolds resolved with Hi-C data confirmed that these blocks of divergence indeed
113 represent inversions (Tigano *et al.* 2021a). Examining how inversions, both in their homozygous and
114 heterozygous states, impact recombination patterns across locally adapted populations is an important
115 next step in understanding the genomic architecture of adaptation. Thanks to the availability of a
116 chromosome-level reference genome and the ability to create lab crosses, we conducted comparative
117 linkage mapping to describe the recombination landscapes of Atlantic silversides within two adaptively
118 divergent populations and their inter-population cross. We first used these maps to anchor large
119 unplaced scaffolds to our previously published silverside genome assembly. We then compared the
120 ordering and genetic distance between markers in the different linkage maps to their physical positions

121 in the genome assembly to identify chromosomal rearrangements and calculate recombination rates.
122 These comparisons allowed us to examine how recombination rates vary across central vs. terminal and
123 inverted vs. uninverted regions of different chromosomes and how recombination differed between
124 sexes and populations.

125

126 Methods

127

128 *Mapping families*

129

130 We generated three crosses for linkage mapping, including two F1 families resulting from reciprocal
131 crossing of wild-caught silversides from two adaptively divergent parts of the distribution range
132 (Georgia and New York), and one F2 family from intercrossing lab-reared progeny from one of the F1
133 families (Figure 1). Because linkage mapping measures recombination during gamete production in the
134 parents, the F1 families give us separate information about the wild-caught male and female founder
135 fish from each separate population (the F0 progenitors), and the F2 map reflects recombination in the
136 hybrid F1 progeny.

137

138 In the spring of 2017, spawning ripe founders were caught by beach seine from Jekyll Island, Georgia
139 (31°03'N, 81°26'W) and Patchogue, New York (40°45'N, 73°00'W) and transported live to the Rankin
140 Seawater Facility at University of Connecticut's Avery Point campus. For each family, we strip-
141 spawned a single male and a single female onto mesh screens submerged with seawater in plastic
142 dishes, then transferred the fertilized embryos to rearing containers (20 l) placed in large temperature-
143 controlled water baths with salinity (30 psu) and photoperiod held constant (15L:9D). Water baths
144 were kept at 20°C for the New York mother and at 26°C for Georgia mother families, which increased
145 hatching success by mimicking the ambient spawning temperatures at the two different latitudes. Post
146 hatch, larvae were provided *ad libitum* rations of newly hatched brine shrimp nauplii (*Artemia salina*,
147 brineshrimpdirect.com). At 22 days post hatch (dph), we sampled 138 full-sib progeny from each of the
148 two F1 families to be genotyped. The remaining offspring from the Georgia-mother F1 family were
149 reared to maturity in groups of equal density (40-50 individuals) in 24°C water baths. In spring 2018,
150 one pair of adult F1 siblings from the Georgia family were intercrossed to generate the F2 mapping

151 population. At 70 dph, we sampled 221 full-sib F2 progeny for genotyping. In total, we analyzed 503
152 individuals: the two founders (male and female) and 138 offspring from each of the two F1 families,
153 plus two additional F1 siblings from the Georgia mother F1 family and their 221 F2 offspring (Fig. 1b).
154 All animal care and euthanasia protocols were carried out in accordance with the University of
155 Connecticut's Institutional Animal Care and Use Committee (A17-043).

156

157 *Genotyping*

158

159 We extracted DNA from each individual with a Qiagen DNeasy tissue kit following the manufacturer's
160 instructions and used double-digest restriction-site associated DNA (ddRAD) sequencing (Peterson *et*
161 *al.* 2012) to identify and genotype single nucleotide polymorphisms (SNPs) for linkage map
162 construction. We created two ddRAD libraries, each with a random subset of ~250 barcoded
163 individuals, using restriction enzymes *MspI* and *PstI* (New England BioLabs cat. R0106S and R3140S,
164 respectively), following library construction steps as in Peterson *et al.* (2012). We size-selected libraries
165 for 400-650 bp fragments with a Pippin Prep instrument (Sage Science) and sequenced the libraries
166 across six Illumina NextSeq500 lanes (75 bp single-end reads) at the Cornell Biotechnology Resource
167 Center.

168

169 Raw reads were processed in Stacks v2.53 (Catchen *et al.* 2013) with the module *process_radtags* to
170 discard low-quality reads and reads with ambiguous barcodes or RAD cut sites. The reads that passed
171 the quality filters were demultiplexed to individual fastq files. To capture genomic regions potentially
172 not included in the current reference genome assembly, we ran the *ustacks* module to assemble RAD
173 loci *de novo* (rather than mapping to the reference genome). We required a minimum of three raw
174 reads to form a stack (i.e., minimum read depth, default *-m* option) and allowed a maximum of four
175 mismatches between stacks to merge them into a putative locus (*-M* option).

176

177 Because the founders contain all the possible alleles that can occur in the progeny (except from any
178 new mutations), we assembled a catalog of loci with *cstacks* using only the four wild-caught F0
179 progenitors. We built the catalog with both sets of founders to allow cross-referencing of common loci
180 across the resulting F1 maps and we allowed for a maximum of four mismatches between loci (*-n*

181 option). We matched loci from all progeny against the catalog with *sstacks*, transposed the data with
182 *tsv2bam* to be organized by sample rather than locus, called variable sites across all individuals, and
183 genotyped each individual at those sites with *gstacks* using the default SNP model (marukilow) with a
184 genotype likelihood ratio test critical value (α) of 0.05. Finally, we ran the *populations* module three
185 times to generate a genotype output file for each mapping cross. For each run of *populations*, we
186 specified the type of test cross (–*map-type* option cp or F2), pruned unshared SNPs to reduce
187 haplotype-wise missing data (–*H* option), and exported loci present in at least 80% of individuals in that
188 cross (–*r* option) to a VCF file, without restricting the number of SNPs retained per locus.

189

190 *Linkage mapping*

191

192 We constructed separate linkage maps for each family using Lep-MAP3 (Rastas 2017), which can
193 handle large SNP datasets and is appropriate for outbred families. For each map (made from a single set
194 of parents and their offspring), we ran the SeparateChromosomes2 module to assign markers into
195 linkage groups using segregation-distortion-aware logarithm of odds (LOD) scores (*distortionLod* = 1),
196 following the author’s recommendations for single family data (Rastas 2018). We tested a range of 10 to
197 25 for LOD score thresholds (*lodLimit*) and evaluated the resulting number of linkage groups and the
198 assignment distribution of markers to each linkage group. The LOD score thresholds were chosen
199 based on variation in size between the largest linkage groups as well as the tail distribution of linkage
200 group size (Rastas 2018). For each map, we chose the smallest LOD threshold at which the largest
201 linkage groups were not further separated and increasing the threshold would instead add smaller
202 linkage groups with few markers while the majority of markers remained in the largest groups.

203

204 Next, we used the *OrderMarkers2* module to order markers and compute genetic distances in
205 centimorgan (i.e., recombination frequency, cM) between all adjacent markers for each linkage group
206 using the default Haldane’s mapping function. We repeated this analysis for each parent in both F1
207 families: we used maternally informative markers (i.e., markers that were heterozygous only in the
208 mother) to estimate recombination between alleles of the F0 female, and paternally informative
209 markers (i.e., markers that were heterozygous only in the father) to estimate recombination between
210 alleles of the F0 male. Lep-MAP3 tends to place difficult-to-order markers (e.g., repeats or errors) at

211 the map ends, which are scaled less to cope with high marker density characteristic of these regions,
212 resulting in long gaps at the ends of some linkage groups. Following recommendations from the author
213 of Lep-Map3, we identified and removed these markers by implementing the trimming script from
214 LepWrap v.3.6.1 (Dimens 2022).

215
216 To investigate sex-specific heterogeneity in recombination, we calculated ratios between female and
217 male total map distances for each linkage group. We then compared our findings to a recent
218 metanalysis of sex-specific recombination rate estimates for 61 fish species (Cooney *et al.* 2021). We
219 replicated their analysis by recalculating map length for males and females as the residuals of the
220 relationship between log10-transformed map lengths and number of markers to control for the effect
221 of marker number on map length estimates.

222
223 Due to strong heterochiasmy, i.e., different recombination rates between the sexes, with male
224 recombination restricted to the terminal ends in most linkage groups (details below), we focused our
225 cross-population comparisons on the female linkage maps in the remainder of the analyses. While we
226 used only maternally informative markers to generate female maps from the two F1 families (Figure 1,
227 red and blue), we used both maternally informative and dually informative markers to get comparable
228 resolution (number of markers) for tracking segregation patterns in the F2 family hybrid mother
229 (Figure 1, yellow). Depending on the genotypes of the F1 individuals sampled to generate the F2
230 family, a marker that was informative in one parent can (i) remain informative, (ii) can become dually
231 informative if two heterozygous F1s were crossed, or (iii) can become uninformative if two
232 homozygous F1s were crossed (Figure S1). As a result, in the F2 family the number of maternally and
233 paternally informative markers is reduced, but some of SNPs that were uninformative in the F1s
234 because the founders were homozygous for different alleles become dually informative for the F2
235 generation.

236
237 *Genome anchoring and improved assembly*
238
239 We aligned the catalog of RAD loci to our recently published silverside reference genome (Tigano *et al.*
240 2021a) using Bowtie2 v2.2.9 (Langmead and Salzberg 2012) with the *--very-sensitive* preset option and

241 converted alignments to BAM output with Samtools v1.11 (Li *et al.* 2009). Using the *Stacks* script
242 *stacks_integrate_alignments*, we generated a table of genome coordinates for SNPs in the catalog BAM
243 file, which we subsequently used to extract the physical positions of markers in the linkage maps.
244 Although the reference genome is largely assembled to chromosome level with a scaffold N50 of 18.19
245 Mb and contains 89.6% BUSCO genes, a number of scaffolds remain unplaced. Therefore, we used the
246 Georgia linkage map (as the reference genome was built with samples from this location) to aid
247 placement of these scaffolds. We anchored and reassembled the silverside genome based on the linkage
248 map with ALLMAPS v1.21 (Tang *et al.* 2015). We assigned previously unplaced genome scaffolds
249 greater than 1 Mb ($n=3$, Tigano *et al.* 2021a) to the 24 largest scaffolds in the reference genome to
250 generate the linkage-map anchored assembly. We renamed chromosomes based on synteny with the
251 medaka genome following Tigano *et al.* 2021a. We also renamed the linkage groups in all the linkage
252 maps based on marker identity to be consistent with renamed chromosomes.

253

254 Analysis of marker order and estimation of recombination rates

255

256 To examine how genetic distance and ordering between markers in the different linkage maps compare
257 to the physical distance on the reassembled chromosomes, we constructed Marey maps that illustrate
258 the position of each SNP in a linkage map against its coordinate in our anchored genome assembly. We
259 initially included all SNPs per RAD-tag to maximize the number of informative markers for linkage
260 mapping, then filtered to retain only one SNP per RAD-tag to reduce redundant data in subsequent
261 analyses. We also removed a small number of outlier SNPs in the Marey map of each chromosome that
262 disrupted the monotonically increasing trend expected from a Marey map function, as these can
263 represent errors in the genetic and/or physical map (Marey maps including the outliers are shown in
264 Figures. S2-S4). By comparing genetic positions from each linkage map to the physical positions in the
265 linkage-map anchored assembly, we identified chromosomal rearrangements as regions containing
266 more than 10 markers with a trend deviating from the linear alignment. We approximated inversion
267 breakpoint locations as the mid-point between the physical coordinates of the markers flanking the
268 edges of identified inverted regions.

269

270 To estimate broad-scale variation in recombination rates for each linkage group in each of the three
271 female maps, we divided the length of each linkage group in cM by the length of the associated scaffold
272 in Mb. To compare recombination rates of the three female maps while accounting for chromosome
273 size, we ran an ANCOVA followed by post hoc analysis with a Bonferroni adjustment. In addition, we
274 used the BREC package (Mansour *et al.* 2021) for estimating local recombination rates in each of the
275 three maps. First, we used the filtered Marey map data to reverse the marker order of regions that are
276 inverted compared to the linkage-map anchored assembly for each of the three female linkage maps.
277 Then, we estimated local recombination rates using the Marey map approach with the linearized
278 markers by correlating genetic and physical maps and fitting a local regression model (Loess with span
279 0.15).

280
281 To compare how fine-scale recombination rates vary between and within chromosomes with and
282 without inversions, we analyzed recombination rates (from the Loess model) using a linear mixed
283 model fit by maximum likelihood with two fixed factors: chromosomal region and mapping family,
284 then used least-square means for post-hoc pairwise comparisons. Due to the non-normal distribution of
285 recombination rates, we first applied a transformation to “Gaussianize” the data using R package
286 LambertW v0.6.6 (Goerg 2015). For this analysis, we compared chromosomes that are collinear among
287 the three female maps (i.e., no inversions) to chromosomes with alternate inversion arrangements in
288 Georgia and New York. We further classified chromosomes into terminal regions (20% of physical
289 length made up of 10% from each end), inverted regions (for chromosomes with inversions), and
290 central regions (not terminal and outside inversions). Statistical analyses were conducted in R v. 3.6.1
291 (Team 2020) using package lme4 (Bates *et al.* 2011).

292
293 *Genomic patterns associated with adaptive divergence*
294
295 We integrated estimates from a forthcoming study of genome-wide differentiation (F_{ST}) between wild
296 populations from New York and Georgia (Tigano *et al.* in prep) to investigate the patterns of
297 differentiation that coincide with structural variants we identified from comparative linkage mapping.
298 F_{ST} was estimated from genotype likelihoods at SNPs in ANGSD v 0.928 (Korneliussen *et al.* 2014) to
299 account for the uncertainty of calling genotypes based on low coverage whole-genome sequencing

300 data, which was generated for 100 individual Atlantic silversides from New York and Georgia
301 populations (n=50 from each site; Wilder et al. 2020). First, we trimmed adapters from the raw data
302 with Trimmomatic (Bolger et al. 2014) and mapped the resulting data to the linkage map anchored
303 assembly with using Bowtie2 v2.2.9 (Langmead and Salzberg 2012) with the --very-sensitive preset
304 option. We calculated the folded site frequency spectrum (SFS) and obtained the maximum likelihood
305 estimate of the SFS for each population, then generated the two-dimensional SFS for the pair of
306 populations, which we used as a prior to estimate pairwise F_{ST} in 10kb windows. Focusing on six
307 chromosomes with the largest inversions identified by comparing the New York linkage map to the
308 Georgia genome, we then superimposed the Marey maps onto the pairwise F_{ST} plots.

309

310

311 Results

312

313 *Genotyping and linkage map construction*

314

315 We obtained 1,840,133,831 raw reads from the 503 silverside samples with an average of 3,658,318
316 reads per sample. After adapter trimming and quality filtering, we retained 1,709,540,728 reads (93%),
317 with an average of 3,398,689 reads per sample. We identified 236,608 loci across all samples, with an
318 average of 45.7% of loci present in each sample (stdev=3.9%, min=0.007%, max=63%), and 19.1x mean
319 per-sample coverage for loci present in the sample (stdev=4.1x, min=6.2x, max=31.2x). Following
320 genotyping and filtering (>80% individuals genotyped per family), we retained 60,671 SNPs across
321 54,937 loci in the Georgia mother F1 family, 64,389 SNPs across 56,028 loci in the New York mother
322 F1 family, and 59,926 variant sites across 54,526 loci in the F2 family.

323

324 Only a subset of the identified SNPs are informative for linkage map construction since linkage can
325 only be determined between markers in which the focal parent has a heterozygous genotype. We were
326 able to use 18,285 female informative and 19,820 male informative markers in the Georgia mother F1
327 family, 20,240 female informative and 19,662 male informative markers in the New York mother F1
328 family, and 20,696 female and dually informative markers in the F2 family. In each of the genetic
329 maps, we obtained 24 linkage groups, consistent both with the haploid number of *M. menidia*

330 chromosomes inferred from karyotyping (Warkentine *et al.* 1987) and the number of putative
331 chromosome clusters identified in both populations with Hi-C data (Tigano *et al.* 2021a). Broadly
332 speaking, the linkage groups are relatively homogeneous in the number of markers across all maps. The
333 total lengths and the number of markers in linkage groups in each of the resulting maps are
334 summarized in Table 1. The edge trimming script identified excessive gaps in two of the linkage groups
335 in the Georgia female linkage map, removing a total of 51 of the 18,285 markers (Figure S5).

336

337 *Sex differences in recombination*

338

339 Comparison of male and female linkage maps reveals conspicuous recombination suppression in males
340 overall, with female maps on average 2.3 times longer than the male maps (Table 1). On all male
341 chromosomes, recombination appears to be restricted to the terminal ends of each chromosome, in
342 most cases to only one end of a chromosome, in both the Georgia male (Figure 3 and S6) and the New
343 York male (Figure S7). Compared to the contrasts in male and female map lengths for 61 fish species
344 (Cooney *et al.* 2021), Atlantic silversides represent one of the most extreme examples of sex-biased
345 recombination rates reported to date (Figure 3). When comparing raw map lengths, the highest
346 female:male ratio (3.59:1) is reported for the Chinook salmon (*Oncorhynchus tshawytscha*; McKinney
347 *et al.* 2016). However, this extreme value is partly attributable to the different number of markers in
348 the male and female maps used in this study, and the signal is tempered when accounting for the
349 difference in number of markers. In the zebrafish (*Danio rerio*), the ratio between female and male
350 map lengths is 2.74 to 1 (Singer *et al.* 2002). After transforming map lengths to account for different
351 numbers of markers, the greatest difference in map lengths is seen in zebrafish, followed by Chinook
352 salmon then Atlantic silversides (Figure 3). In contrast to our male maps, our female maps show
353 extensive recombination across the entire length of each chromosome, so we focus on the female maps
354 for the analysis of synteny and recombination rate variation. Among the female linkage maps, we
355 found the largest map length in the New York female (3869 cM) compared to the Georgia female (3553
356 cM) and the inter-population hybrid female (3555 cM).

357

358 *Linkage map anchored assembly*

359

360 After edge trimming and considering only one SNP per RAD locus, we were left with 12,751 of the
361 initial 18,285 SNPs used to build the Georgia female linkage map. Of these, 11,102 (87.1%) mapped to
362 one of the main 24 scaffolds in the published genome assembly, 186 (1.5%) mapped to three additional
363 scaffolds (>1 Mb), 833 (6.5%) mapped to smaller unplaced scaffolds, and 630 (4.9%) did not map to any
364 sequence in the reference genome assembly (Figure 4 and S2).

365 We used these mappings to anchor and order unplaced scaffolds into chromosome-scale
366 pseudomolecules. We are able to anchored the three unplaced long scaffolds (> 1 Mb) to the linkage-
367 map guided assembly, adding 15.4 Mb of sequence to the chromosome assembly. Two of these
368 scaffolds, encompassing 7.8 and 4.7 Mb, were added to the beginning of chromosome 1, and the third,
369 encompassing 2.8 Mb, was added to the beginning of chromosome 24 (Figure S8).

370

371 *Analysis of female map order*

372

373 Comparison of the female linkage maps to the improved reference genome reveals chromosomal
374 rearrangements in all three maps (Figure 5). Our reference genome was assembled from an individual
375 from Georgia, and while the Georgia female linkage map shows high levels of collinearity with the
376 reference genome sequence as expected, we also see evidence of inversions (reversal of marker
377 ordering in the linkage map compared to the physical sequence). We detected five inversions in the
378 Georgia female linkage map: 0.4 Mb at the beginning of chromosome 1, 1.5 Mb at the end of
379 chromosome 5, 0.9 Mb toward the beginning of chromosome 10, 1.4 Mb toward the beginning of
380 chromosome 12, and 2.1 Mb at the beginning of chromosome 19 (Figure 5). Four of these five
381 inversions (on chromosomes 1, 5, 10, and 12) also appear in the New York and F2 family maps. While
382 an inversion appearing in all maps could suggest misassembled regions in the reference genome, these
383 populations are known to harbor polymorphic inversions, making it difficult to discern structural
384 variants from potential misassemblies in this instance. We did identify three seemingly misassembled
385 regions, at the end of chromosome 10, and at the beginnings of chromosome 20 and 24. These regions,
386 in addition to displaying alternate orientations, also create gaps in the genetic map and additional data
387 will be needed for their accurate placement. Moreover, a striking pattern of complete recombination
388 suppression across a wide region (flatlining in genetic distance across > 10 Mb of the physical genome
389 sequence) is seen on chromosomes 6 and 19 of the Georgia female linkage map. These regions may be

390 the signature of inversions that segregate in the Georgia population for which the sampled female was
391 heterozygous.

392

393 When comparing the New York female linkage map to the Georgia reference genome sequence, we
394 detected a total of 13 chromosomal inversions across 10 of the 24 chromosomes. The inversions range
395 in size from 0.4 to 12.5 Mb, with the largest spanning much of the length of chromosome 8. The
396 majority of chromosomes 18 and 24 are also inverted, with the former having three adjacent inversions
397 at positions 0.9-1.5 Mb, 1.5-4.2 Mb, and 4.2-8.4 Mb, and the latter having the second largest inversion
398 that captures 9.3 Mb (Figure 5). Smaller inversions are seen on chromosome 1 (at position 1.6-2 Mb),
399 chromosome 4 (at position 12.7-14.7 Mb), chromosome 7 (at position 11.8-13.6 Mb), and chromosome
400 19 (at position 2.9-4.2 Mb). In all, these rearrangements span 38.6 Mb, or 8.3% of the 465.7 Mb
401 chromosome assembly (i.e., the 24 largest scaffolds of the genome).

402

403 The F2 family map reveals the effect of these inversions on the recombination landscape in crosses
404 between New York and Georgia (because it reflects meiotic recombination in an F1 daughter with a
405 wild-caught parent from each of these populations). As expected, chromosomal regions with opposite
406 orientations of inversions between these two populations do not recombine in the heterozygous
407 offspring, as revealed by the flatlining of genetic map distances in those regions (Figure 5, yellow data
408 points). Chromosomes 8, 18, and 24, which were previously identified as harboring highly divergent
409 haplotypes in the two studied populations (Wilder *et al.* 2020), show large blocks of suppressed
410 recombination in the hybrid mother of the F2 family map as a result of the inversions. In chromosome
411 18, recombination is suppressed an additional 1.8 Mb beyond the inversions identified (at position 8.4-
412 10.2 Mb, Figure 5).

413

414 Recombination was also suppressed on chromosome 11 in the hybrid female map without evidence of
415 an inversion between the two parental maps in this position. Chromosome 11 was, however, also
416 previously identified as having a large block of SNPs in tight LD and nearly fixed for opposite alleles
417 across the range, supporting the presence of an inversion in this genomic location. To note, highly
418 divergent northern haplotypes associated with this inversion were most common in locations further
419 north (Gulf of Maine and Gulf of Saint Lawrence) of the populations sampled in this study (Wilder *et*

420 *al.* 2020). While the southern haplotype on chromosome 11 is predominant in both Georgia and New
421 York, the northern haplotype is present in low frequency in New York. Thus, the suppression of
422 recombination in this region of chromosome 11 in the F2 map may be the signature of an inversion
423 that segregates in the New York population, but did not show up in our F1 New York map because the
424 female used to establish the New York map (F1) carried the southern arrangement (collinear with the
425 assembly). A northern (inverted) haplotype was likely introduced by the New York male that became
426 the grandfather of our F2 offspring (see Figure 1), explaining how the F2 offspring became
427 heterozygous for this region. In a similar vein, the recombination suppression seen on chromosome 6
428 in the Georgia female linkage map is also seen on the F2 family map, while the suppression on
429 chromosome 19 is not, again likely reflecting signatures of inversions that segregate within
430 populations. These four regions of suppressed recombination on Chromosomes 6, 11, 18, and 19
431 representing putative inversion heterokaryotypes span an additional 33.9 Mb of the chromosome
432 assembly.

433

434 *Estimation of recombination rates*

435

436 As evident from the Marey maps in Figure 5, estimated female recombination rates vary across the
437 genome (Figure 6). We observe increased rates of recombination near the ends of many (but not all)
438 chromosomes and reduced recombination towards the centers, often with drops to near zero, in what
439 are likely centromere regions. While there is a significant negative relationship ($R = -0.39$, $p < 0.001$)
440 between chromosome size and average recombination rate in all three maps analyzed together, this
441 trend is non-significant when analyzed for each map separately (Figure 7a). Recombination rates vary
442 among maps ($F = 6.78$, $df = 2,68$, $p < 0.001$), with significantly higher mean recombination rates in New
443 York (7.59 cm/Mb, 95% CI [7.27, 7.91]) compared to the Georgia (6.98 cm/Mb, 95% CI [6.66, 7.30])
444 and hybrid F1 (6.80 cm/Mb, 95% CI [6.48, 7.12]) female maps, but no significant difference between
445 the latter two (Figure 7a). Chromosomes with and without inversions show no difference in average
446 recombination rate ($z = 0.253$, $p = 0.80$). Variation in fine-scale recombination rates (from the Loess
447 model) is evident across terminal, central, and inverted regions of chromosomes with and without
448 inversions (Figure 7b). ANOVA with Satterthwaite's method revealed significant differences in
449 recombination rates related to population ($F = 430.2$, $df = 2$, $p < 0.001$), chromosomal region ($F =$

450 1213.4, $df = 3$, $p < 0.001$), and their interaction ($F = 305.3$, $df = 6$, $p < 0.001$). Recombination rates are
451 higher in the terminal ends of all chromosomes, regardless of the presence of inversions. Inverted
452 regions, however, have lower recombination rates compared to regions outside inversions in
453 chromosomes with inversions as well as compared to central regions in chromosomes without
454 inversions. While this pattern is primarily driven by the reduced recombination in inversions in the
455 hybrid map, when considering only the F1 family maps, recombination rates inside inversions are still
456 lower than regions outside inversions ($z = 9.66$, $p < 0.0001$) but no different than the central regions of
457 chromosomes without inversions ($z = 1.245$, $p = 0.43$).

458

459 *Genomic patterns associated with adaptive divergence*

460

461 Large inversions coincide near perfectly with blocks of highly elevated differentiation between
462 between populations from New York and Georgia (Figure 8).

463

464

465 Discussion

466

467 By building and comparing multiple high-density linkage maps, we found remarkable variation in
468 recombination patterns between both sexes and across adaptively divergent populations of the Atlantic
469 silverside. We also validated standing variation in large-scale chromosomal inversions and
470 demonstrated how these inversions suppress recombination in heterozygous individuals.

471

472 *Suppressed recombination in males*

473

474 We showed that the recombination landscape in the Atlantic silverside varies substantially both within
475 and across chromosomes, and between sexes and populations, a pattern that is consistent with other
476 study systems (Kong *et al.* 2010; Smukowski and Noor 2011; Sardell and Kirkpatrick 2020). Males
477 showed virtually no recombination across central portions of all chromosomes (Figure 2). The
478 restriction of recombination to telomeric regions in males has also been demonstrated in other species
479 with female-biased heterochiasmy, which is more common than homochiasmy in animals (Brandvain

480 and Coop 2012; Sardell and Kirkpatrick 2020). We found that the two F1 family female maps are on
481 average 2.3 times longer than the male maps, one of the most sex-biased recombination rates known
482 for fishes (Figure 3).

483

484 A recent metanalysis compared sex-specific recombination rates in 61 fish species, concluding that sex
485 differences in recombination rate are evolutionary labile, with frequent shifts in the direction and
486 magnitude of heterochiasmy that cannot be explained by neutral processes or biological sex differences
487 in meiosis (Cooney *et al.* 2021). Alternative hypotheses include the Haldane-Huxley hypothesis, which
488 posits that recombination may be adaptively suppressed to varying degrees across the genome in the
489 heterogametic sex, in order to prevent X-Y or Z-W crossing over (Haldane 1922; Huxley 1928).
490 However, this probably does not apply to silversides, which exhibit partial environmental sex
491 determination (Conover and Kynard 1981; Duffy *et al.* 2015) and do not appear to have heteromorphic
492 sex chromosomes (Akopyan, unpublished data). In addition, there is no significant correlation between
493 sex determination mechanism and sex-bias in recombination rate across fish species (Cooney *et al.*
494 2021). Other hypotheses relate to sexual selection and sexual conflict, predicting that patterns of
495 heterochiasmy are a result of stronger selection experienced by one sex or their gametes (haploid
496 selection), but the data to test this are currently lacking for most fish species (Cooney *et al.* 2021). In
497 silversides, partial sexual size dimorphism has been previously documented, with slower growing males
498 experiencing higher size-selective mortality compared to females (Pringle and Baumann 2019). While
499 this is in line with predictions of the sexual conflict hypothesis, which favors suppressed
500 recombination in the sex subject to stronger selection (Sardell and Kirkpatrick 2020), further
501 investigation is warranted to characterize the relationship between sexual conflict and sex-biased
502 recombination rates in silversides.

503

504 *Recombination landscapes in females*

505

506 In the female maps, we found a weak negative correlation between recombination rates and
507 chromosome size, a pattern that is common but not ubiquitous among other species (Stapley *et al.*
508 2017). As genome size predicts variation in chromosome size (Li *et al.* 2011) and chromosomes of
509 different sizes tend to experience different recombination rates (Haenel *et al.* 2018), a weak negative

510 correlation is expected based on the relatively small genome size of the Atlantic silverside (Tigano *et al.*
511 2021b). We also discerned differences in fine-scale recombination rates along the genome (Figure 6
512 and 7), including elevated recombination at the terminal ends of chromosomes, and suppressed
513 recombination in central regions, consistent with patterns in a large variety of taxa (Haenel *et al.* 2018;
514 Peñalba and Wolf 2020).

515
516 Looking across populations, we found a tendency for higher average recombination rates in the New
517 York female map compared to both the Georgia and hybrid maps (Figure 7a). Variation in
518 recombination rates among individuals and populations is well-established, but we still have a limited
519 understanding of the underlying patterns and drivers. Recent work examining *Drosophila* populations
520 demonstrated that natural selection can shape interpopulation differences in recombination rate
521 (Samuk *et al.* 2020). The two F1 maps in our study gave us a first glimpse into the within-species
522 variation in recombination patterns in Atlantic silversides, but because each map is based on just a
523 single female, we cannot confidently disentangle whether the differences are driven by variation
524 among individuals vs. consistent variation among populations. Interestingly, the New York mother
525 family was raised at a lower temperature than the Georgia mother family. Increased temperatures are
526 known to elevate recombination rates (Plough 1917; Elliott 1955), so the higher recombination rate in
527 the New York map could reflect an underestimation of true differences. However, further study is
528 needed to determine how temperature affects recombination in silversides and a more comprehensive
529 investigation of recombination patterns across the species range is needed to determine the geographic
530 distribution of this variation.

531

532 *Chromosomal inversions*

533
534 We detected a total of 13 chromosomal inversions across 10 of the 24 chromosomes. These inversions
535 range in size from 0.4 to 12.5 Mb and in total span 38.6 Mb or 8.3% of the silverside genome. We
536 detected four additional putative inversions, presumably heterozygous in the Georgia and hybrid maps,
537 ranging in size from 1.8 to 12.9 Mb and together span an additional 33.8 Mb or 7.3% of the silverside
538 genome. Overall, these rearrangements span 72.4 Mb, or 15.6% of the 465.7 Mb chromosome assembly.
539 These findings add to a growing body of studies that implicate inversions as important drivers of

540 evolutionary change. A powerful mechanism for protecting co-adapted alleles from dissociation, large
541 inversions are widespread and typically span many genes: a recent review showed that the average
542 reported inversion size in both plants and animals is 8.4 Mb, ranging from 130 kb to 100 Mb, and
543 contain an average of 418 genes (Wellenreuther and Bernatchez 2018). Here, we identified a subset of
544 the 662 inversions affecting 23% of the genome recently reported to be segregating between southern
545 and northern populations of Atlantic silversides, inferred from alignment of independent genome
546 assemblies (Tigano *et al.* 2021a). Our study, which provides independent evidence that clearly confirms
547 the presence and impact of the larger inversions detected in the genome (especially those on
548 chromosomes 8, 11, 18, and 24), certainly underestimates the total number of rearrangements in the
549 silverside genome. This is a reflection of the ascertainment bias of reduced genome representation
550 methods (such as the RAD genotyping used here), which only have the resolution to detect relatively
551 large inversions. In addition, linkage mapping can be biased by the individuals used to establish a
552 pedigree; a single pedigree cannot fully capture the full set of inversions segregating in a focal
553 population, and we only observe inversions that are variable among our specific founding individuals.
554 Moreover, linkage mapping only considers recombination events in gametes that resulted in viable
555 offspring and does not characterize recombination in unsuccessful gametes. However, our pedigree-
556 based approach provides a direct estimate of genetic linkage by observing the inheritance of alleles in a
557 few families, allowing us to robustly distinguish recombination rates among individuals of the parental
558 generation, including the different sexes and populations. Compared to population-based inferences
559 (for estimating recombination and detecting inversions), genetic maps are affected to a much lesser
560 extent by demography and selection acting across evolutionary times and provide a key resource for
561 future comparative genomic and QTL studies in this species (Sarropoulou and Fernandes 2011; Samuk
562 and Noor 2021).

563

564 *Genomic patterns associated with adaptive divergence*

565

566 Structural variation within the genome can promote genomic divergence by locally altering
567 recombination rates. The key evolutionary effect of inversions is that they suppress recombination in a
568 heterozygous state (Sturtevant and Beadle 1936). This study demonstrated that inversion
569 polymorphisms between locally adapted Atlantic silverside populations suppress recombination in

570 inter-population hybrids. Suppressing recombination is an efficient way to preserve linkage between
571 favorable combinations of locally adapted alleles but is advantageous only when populations
572 experience gene flow (Faria *et al.* 2019b). Populations of the Atlantic silverside south of Cape Cod
573 (including both Georgia and New York) show high connectivity across this broad geographic range
574 that spans the steep latitudinal temperature gradient of the North American Atlantic coast (Lou *et al.*
575 2018; Wilder *et al.* 2020). Hatching in the intertidal zone in the spring, silversides move up to 170-km
576 offshore to overwinter (Conover and Murawski 1982), and extensive mixing between spawning sites
577 has been documented (Clarke *et al.* 2009; Wilder *et al.* 2020). The discovery of chromosomal
578 rearrangements that suppress recombination between populations suggests a possible mechanism that
579 could preserve the association between locally favorable alleles and as such help maintain
580 combinations of locally adaptive traits (Therkildsen *et al.* 2019).

581

582 Inverted regions coincide near perfectly with blocks of strongly elevated differentiation. Larger
583 inversions (e.g., on chromosomes 8 and 24) show a concave pattern with elevated differentiation at the
584 breakpoints, which may be due to stronger divergent selection associated with breakpoints (Villoutreix
585 *et al.* 2021), and/or higher levels of gene flux and mutations with increasing distance from the
586 breakpoints (Andolfatto *et al.* 2001). The co-location of blocks of highly elevated differentiation
587 provides strong evidence that divergent selection favors opposite orientations of the large inversions in
588 different populations and suggests that they play an important role in enabling adaptive divergence
589 despite gene flow in Atlantic silversides.

590

591 Inversions can capture alleles that control adaptive traits into a single complex block to prevent their
592 dissociation by reducing recombination in heterokaryotypes, while the majority of the genome is
593 homogenized by gene flow. Although we saw no recombination within the large inversions among the
594 221 offspring examined here, the recombination suppression in heterokaryotypes, however, is not
595 necessarily complete on a population scale because viable recombinant gametes may arise by double
596 crossing over or by gene conversion (Sturtevant and Beadle 1936; Chovnick 1973), but this tends to
597 occur at low rates. Furthermore, inversion polymorphisms are not static, but continue to evolve after
598 establishment. Inversion dynamics are thus complex and depend on the relative roles of selection, drift,

599 mutation, and recombination, all of which change over time and have implications for the inversion
600 itself and the evolution of the populations (Faria *et al.* 2019b).

601

602 An outstanding question regarding the role of inversions in adaptive evolution is whether they become
603 targets of strong selection because of their content or because they generate mutations or gene
604 disruptions at breakpoints (Kirkpatrick 2010; Wellenreuther and Bernatchez 2018). Previous work has
605 shown that linked genes in the major inversion regions are enriched for functions related to multiple
606 local adaptations in silversides: gene sets in outlier sections of chromosome 8, 18, and 24 have been
607 shown to be enriched for gene ontology terms related to polysaccharide metabolic processes, meiotic
608 cell cycle, cartilage morphogenesis, regulation of behavior, and regulation of lipid storage, and these
609 functions all relate to traits that show adaptive divergence in this species (Wilder *et al.* 2020). This
610 functional enrichment could suggest that gene content may play an important role in the origin and
611 maintenance of inversions and could indicate that the inversions may act as supergenes to maintain
612 coinheritance of adaptive alleles. An important aspect of supergenes is that they allow switching
613 between discrete complex phenotypes and can maintain stable local polymorphism without the
614 generation of maladaptive intermediates (Thompson and Jiggins 2014). While we have evidence from
615 our linkage maps that some structural variants are polymorphic within populations (e.g. inversions on
616 chromosome 6 and 19 in Georgia and on chromosome 11 in New York), determining whether
617 inversions are indeed acting as supergenes requires further work to disentangle phenotype-genotype
618 association and examine their frequencies within and among populations, as well as to rule out
619 alternative hypotheses (e.g., inversions disrupt associations of gene-regulatory elements).

620

621

622 Acknowledgements

623

624 We thank Harmony Borchardt-Wier for help with DNA extractions, Steve Bogdanowitz for help with
625 preparation of the RAD-seq libraries, Pasi Rastas for discussions and advice on implementing and
626 interpreting Lep-Map3 analyses, Pavel Dimens for advice on implementing Lep-Wrap, and members of
627 the Therkildsen lab for their thoughtful feedback on the manuscript. This study was funded through a
628 National Science Foundation grant to NOT (OCE-1756316) and OCE-1756751 to HB.

629
630 Data Accessibility
631
632 Raw data from the RADseq libraries will be available under NCBI BioProject accession number
633 PRJNA771889. Scripts for all analyses will be available at <http://github.com/therkildsen-lab/silverside-linkage-maps>
634

635 Tables

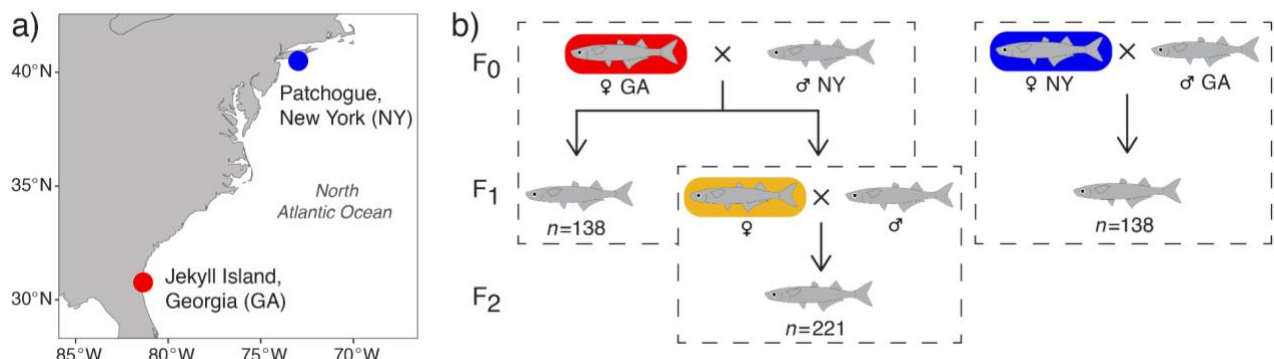
636

637 Table 1. Summary of the total lengths (in cM) and number of SNPs assigned to the different linkage
638 groups (LG) in each of the male and female linkage maps. Downstream analyses that compare linkage
639 map positions to the physical position of markers in the genome sequence are based only on the subset
640 of markers shown here that map to the genome assembly, survived manual outlier removal, and
641 include only one SNP per RAD locus (map lengths and SNP counts retained for analysis are shown in
642 Table S1).

LG	Female						Male			
	Georgia		New York		F1		Georgia		New York	
	cM	SNPs	cM	SNPs	cM	SNPs	cM	SNPs	cM	SNPs
1	150.9	784	170.9	928	170.0	886	112.7	887	88.8	870
2	121.0	444	118.9	513	138.8	339	58.0	432	30.4	416
3	178.5	924	202.0	1033	128.3	1102	63.9	1024	69.9	1093
4	152.3	988	155.0	998	127.7	1190	68.8	995	54.9	1019
5	177.5	934	204.8	1038	178.5	1034	69.6	986	63.9	943
6	118.1	995	160.6	1093	150.7	887	72.1	1011	52.7	1064
7	169.9	1021	174.9	1020	176.4	1025	49.8	1043	54.6	1027
8	138.6	523	162.1	873	109.9	1109	57.6	1144	57.9	943
9	165.3	755	181.5	832	173.4	829	75.0	817	74.1	876
10	146.4	859	165.5	887	158.5	856	61.7	867	50.3	839
11	158.9	772	160.8	983	147.3	1061	49.9	1033	53.3	959
12	149.1	710	163.5	811	156.1	747	58.7	775	53.6	759
13	153.4	874	160.4	894	155.9	880	88.1	851	79.8	845
14	138.7	791	158.7	856	146.0	923	54.6	856	60.6	811
15	155.5	799	177.3	837	175.9	842	60.5	796	102.7	816
16	169.3	830	187.2	899	131.1	597	63.5	912	80.8	906
17	125.5	716	146.7	809	144.7	806	63.1	774	59.5	780
18	110.3	440	141.6	559	126.4	920	60.8	526	60.8	460
19	110.2	665	145.7	770	152.2	622	62.3	685	55.2	670
20	125.9	638	131.8	700	142.0	688	55.9	644	51.4	706
21	146.7	777	152.2	785	148.7	836	66.5	721	60.2	781
22	156.7	807	162.5	848	166.0	521	76.7	797	67.6	778
23	139.2	620	122.9	622	126.0	736	81.2	620	66.7	657
24	195.6	619	162.3	652	124.1	1260	116.1	624	61.3	644
Total	3553	18285	3869	20240	3555	20696	1647	19820	1511	19662

643

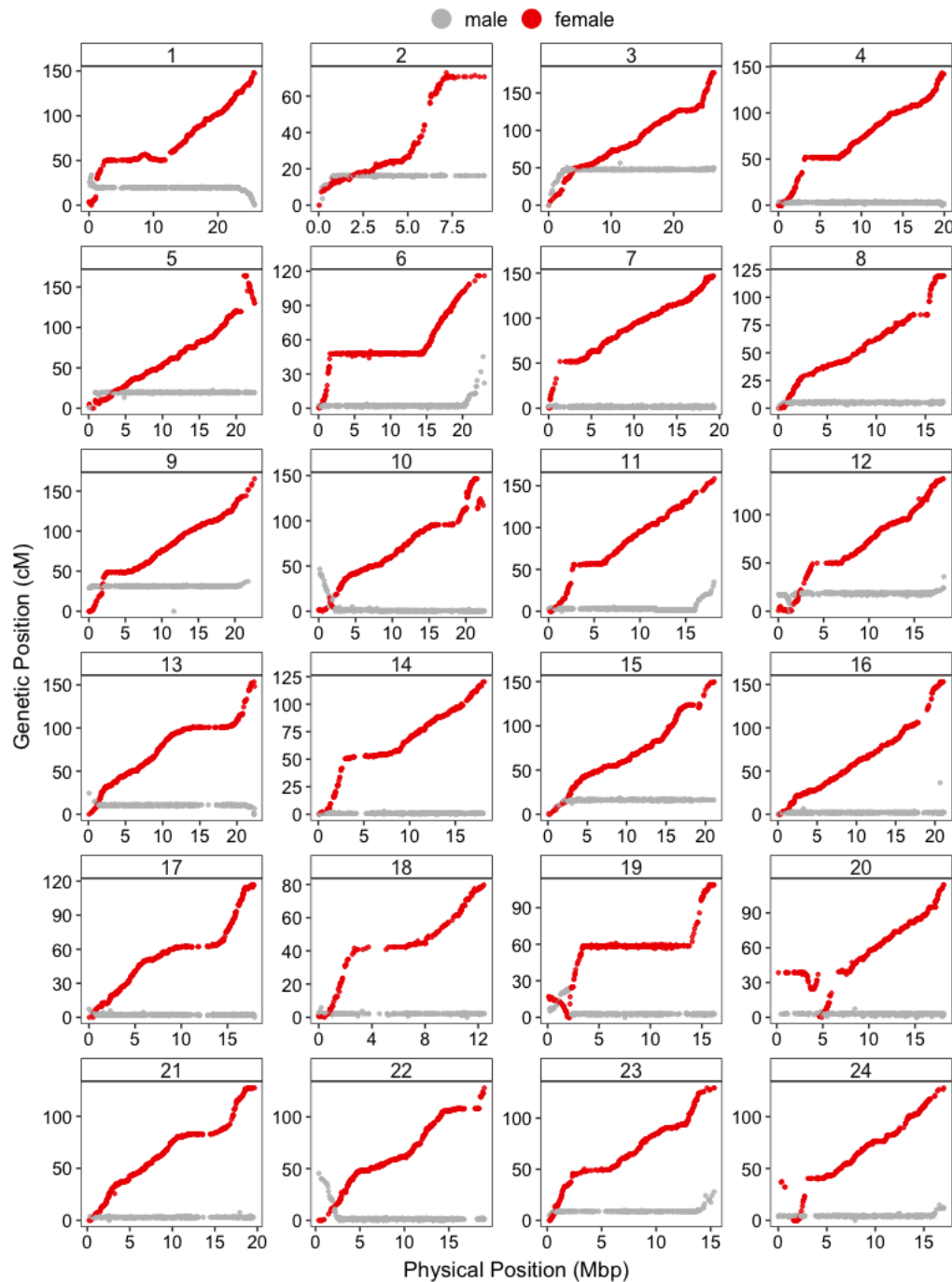
644 Figures



645

646 Figure 1. Experimental Design

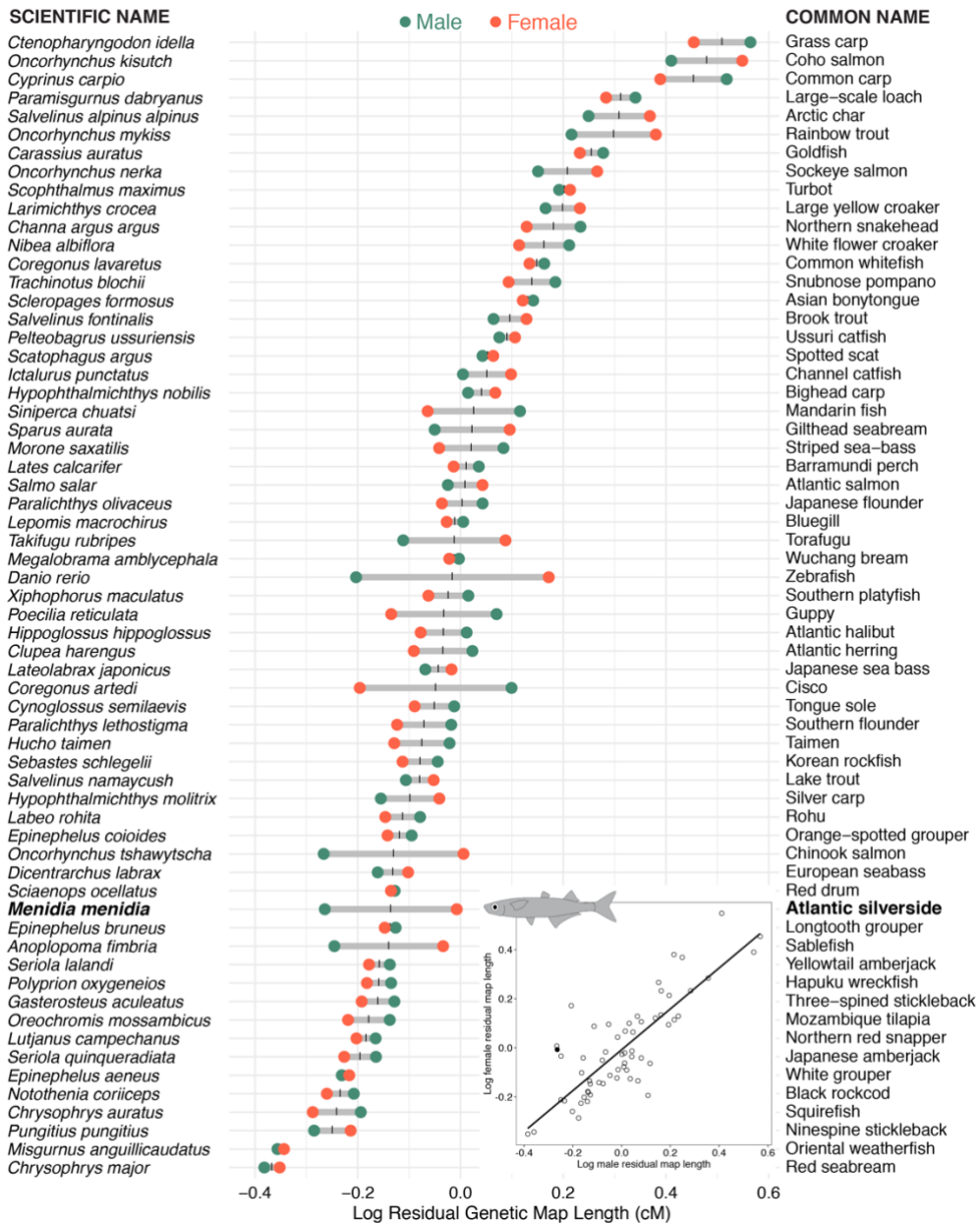
647 Map of sampling localities of wild-caught F0 individuals from Jekyll Island, Georgia and Patchogue,
648 New York (a) used for generating mapping families created according to the diagram shown in panel b.
649 Each dashed box represents a family for which we produce a linkage map and the number of offspring
650 (n) analyzed in each family is labeled. Focal females used for population comparisons are colored to
651 match Figures 5-7 (and sampling localities in the founders).



652

653 Figure 2. Male and Female Marey Maps

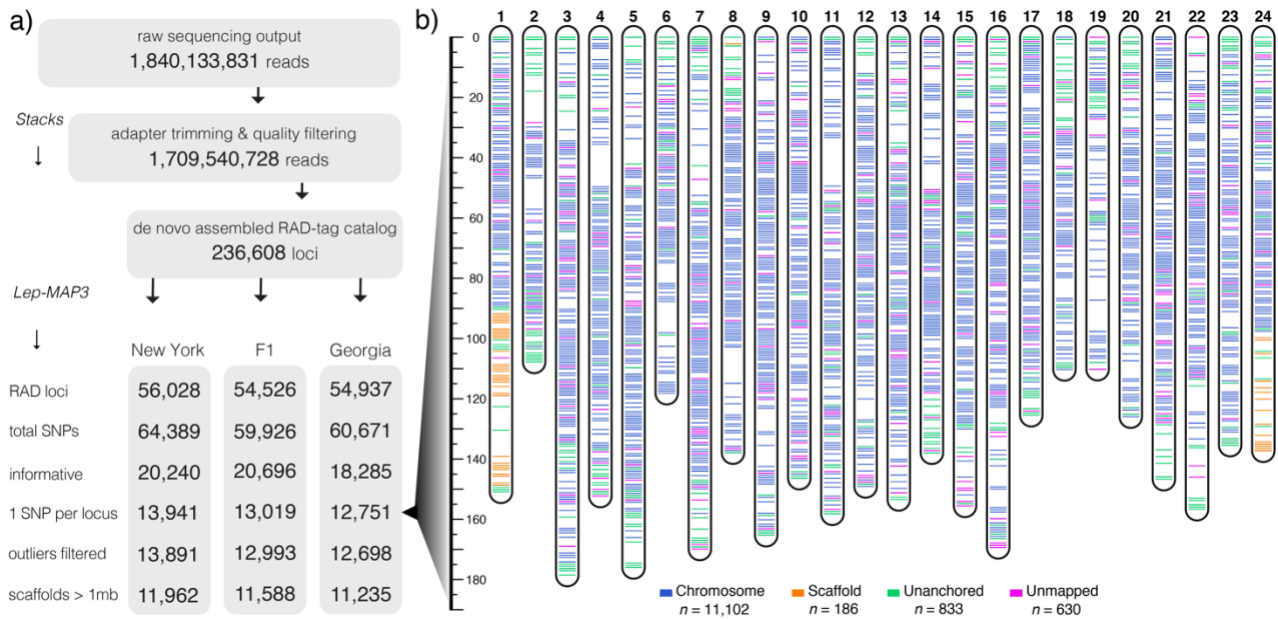
654 The genetic map position (cM) vs. the physical position in the genome sequence of the SNPs assigned
 655 to each chromosome for the male and female from Georgia reveals extreme heterochiasmy, with male
 656 recombination restricted to the terminal ends in most linkage groups. These plots include only one
 657 SNP per RAD locus that maps to the reference genome (unfiltered male maps are shown in Figures S6
 658 and S7).

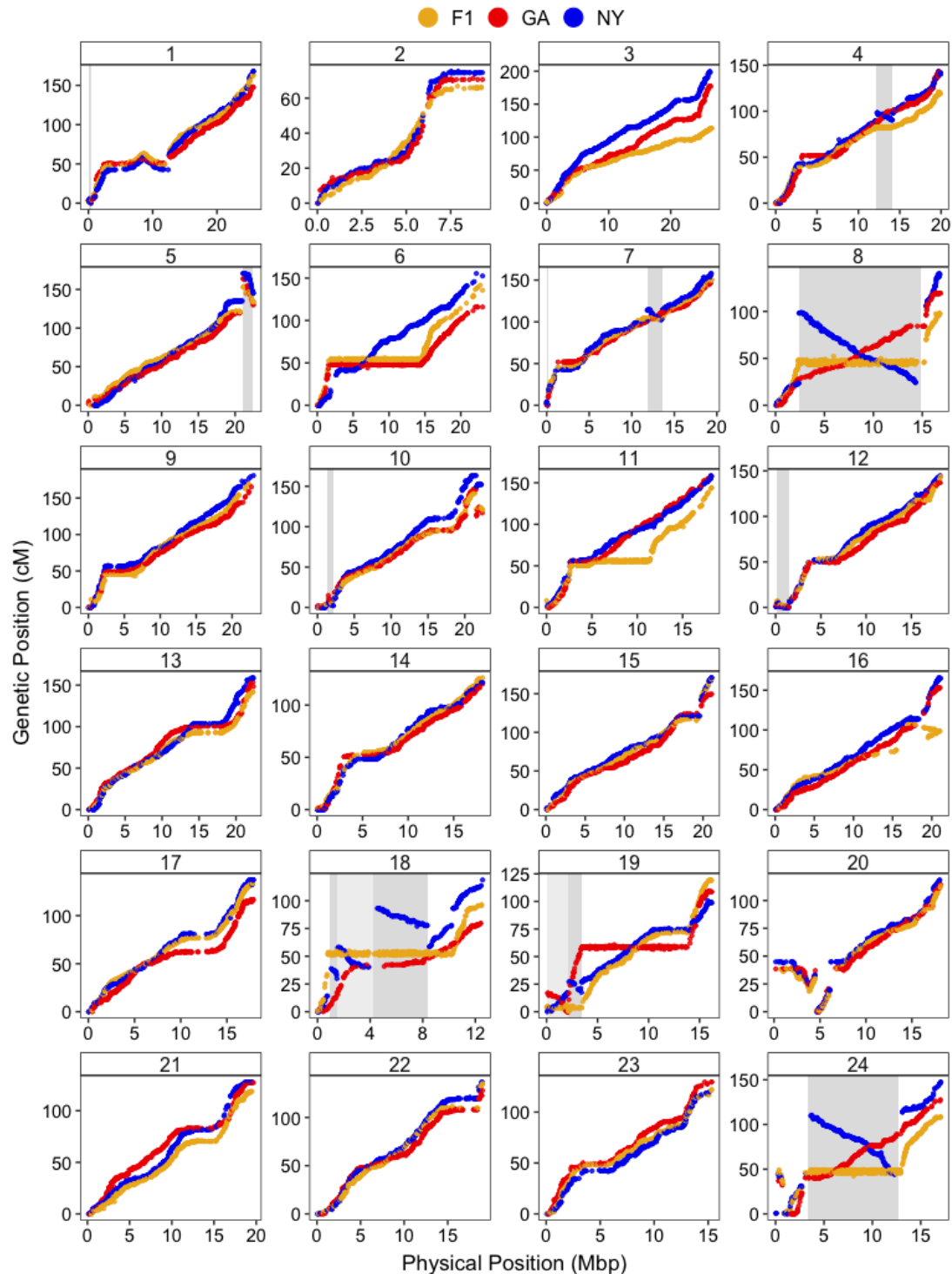


659

660 Figure 3. Heterochiasmy in Fishes

661 Atlantic silversides have one of the highest differences between female and male map lengths
 662 compared to 61 fish species reviewed by Cooney *et al* 2021. For each species listed, map length after
 663 accounting for variation in numbers of markers is shown in green for males and orange for females.
 664 Grey horizontal bars represent the difference between the sexes and the vertical black bars indicate the
 665 sex-averaged map length, which was used to order species along the y-axis. The inset plot represents
 666 the relationship between male and female map lengths for all the species, where the Atlantic silverside
 667 (closed circle) shows considerable deviation from a one-to-one ratio.



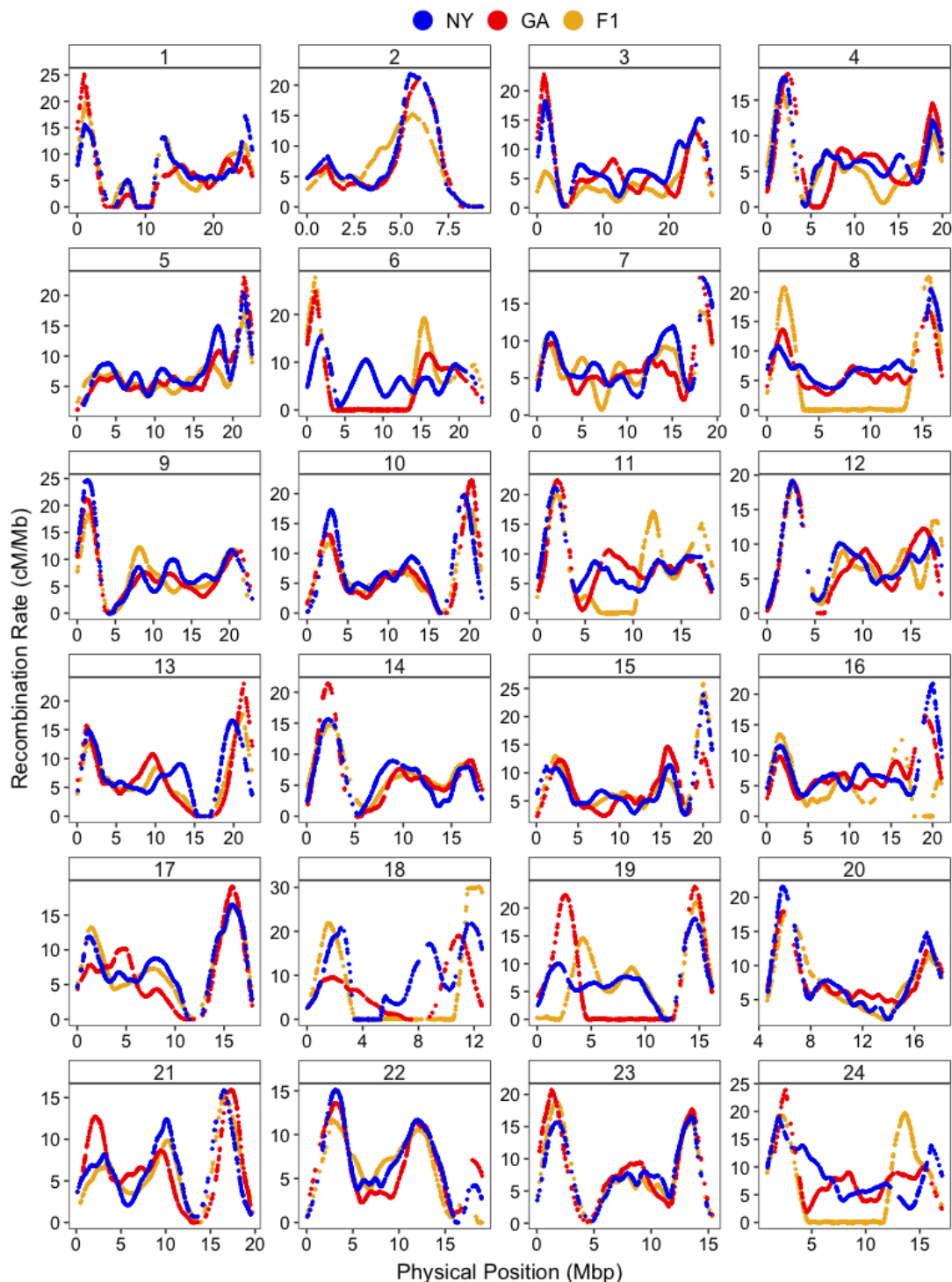


677

678 Figure 5. Female Marey Maps

679 Genetic distance (cM) along the physical distance (Mb) of each chromosome is shown for all three
 680 females. Each point is a SNP and the marker order in the GA female is shown in red, NY in blue, and

681 their resulting hybrid in yellow. Shaded regions highlight inversions with alternate arrangements in
682 the GA and NY female.



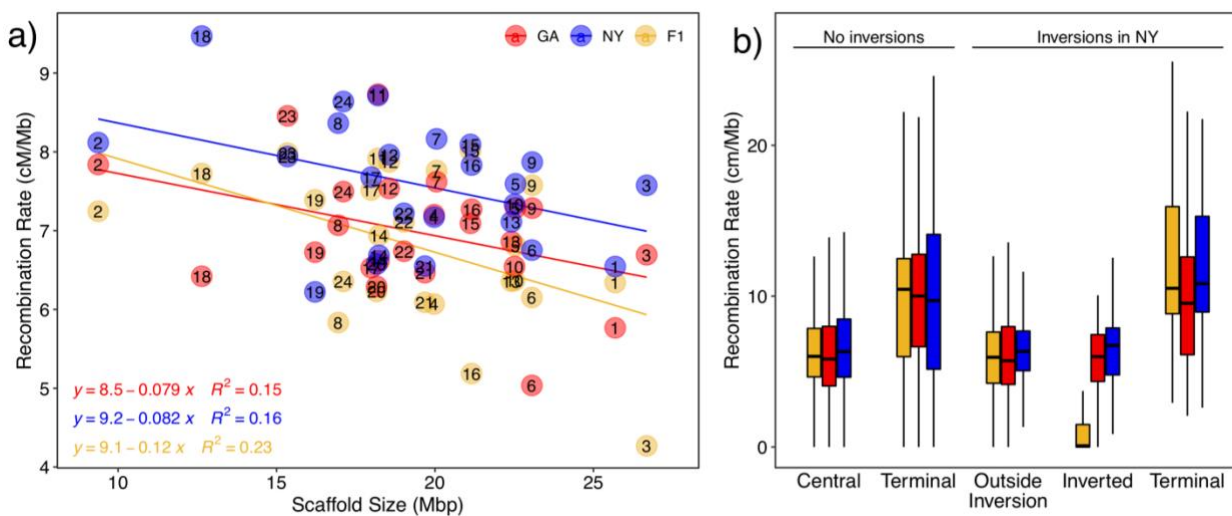
683

684 Figure 6. Female Recombination Maps

685 Fitted splines represent the variation in recombination rate as a function of physical distance for the
 686 three mapping families. The maps show that most chromosomes have a region (presumably the

687 centromere) where recombination is close to zero in all females and that this region tends to be offset
688 from the center of the chromosome.

689



690

691 Figure 7. Comparing Recombination Rates

692 a) A comparison across all chromosomes reveals a tendency for higher averaged recombination rates in
693 smaller chromosomes in all three maps, and overall significantly higher recombination rates across
694 chromosomes in NY. b) Across the maps, recombination rates are higher in the terminal ends (10% of
695 each end) of all chromosomes, both those with and without inversions. As expected, the inversions
696 show no recombination in the F1 female that was heterozygous for those regions (yellow), but the
697 inverted regions also have lower recombination rates in both homozygotes (GA and NY shown in blue
698 and red) compared to regions outside inversions.

699

700

701

702

703

704

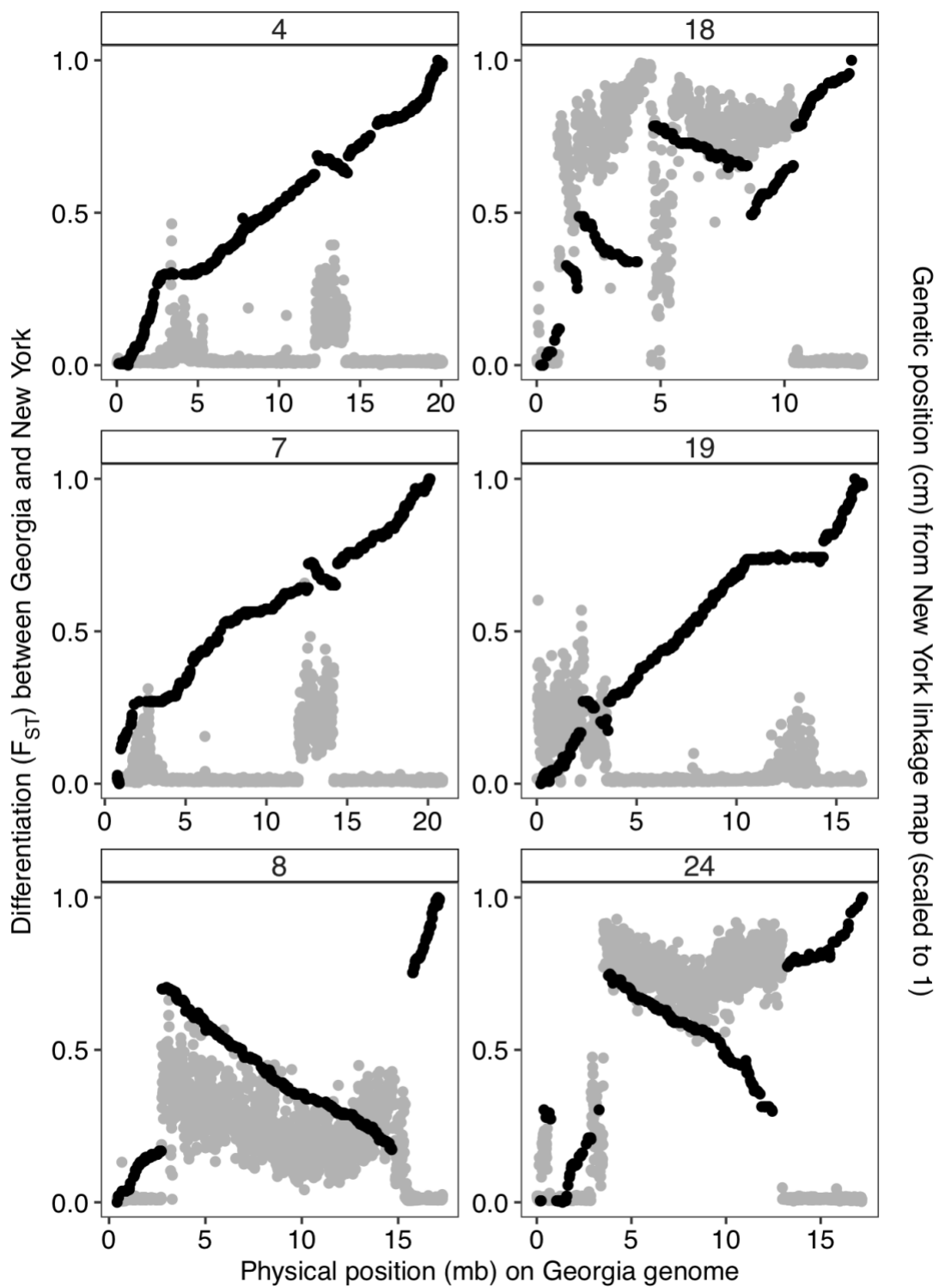
705

706

707

708

709
710
711
712



714 **Figure 4.** Inversions coincide with patterns of genomic differentiation between populations. Gray
715 points show F_{ST} in 10kb windows between the wild populations (left y-axis), and black points show
716 how the genetic positions (in centimorgan) from the New York linkage map (right y-axis) compare to
717 the Georgia genome.

718 References

719 Altenberg L., and M. W. Feldman, 1987 Selection, generalized transmission and the evolution of
720 modifier genes. I. The reduction principle. *Genetics* 117: 559–572.
721 <https://doi.org/10.1093/genetics/117.3.559>

722 Anderson L. K., A. Lai, S. M. Stack, C. Rizzon, and B. S. Gaut, 2006 Uneven distribution of expressed
723 sequence tag loci on maize pachytene chromosomes. *Genome Res* 16: 115–122.
724 <https://doi.org/10.1101/gr.424990>

725 Andolfatto, P., F. Depaulis, and A. Navarro, 2001 Inversion polymorphisms and nucleotide variability
726 in *Drosophila*. *Genetics Research*, 77: 1-8. <https://doi.org/10.1017/S0016672301004955>

727 Arnott S. A., S. Chiba, and D. O. Conover, 2006 Evolution of intrinsic growth rate: metabolic costs
728 drive trade-offs between growth and swimming performance in *Menidia menidia*. *Evolution* 60:
729 1269–1278. <https://doi.org/10.1111/j.0014-3820.2006.tb01204.x>

730 Barton N. H., and B. Charlesworth, 1998 Why sex and recombination? *Science* 281: 1986–1990.
731 <https://doi.org/10.1126/science.281.5385.1986>

732 Bates D., M. Maechler, B. Bolker, S. Walker, R. H. B. Christensen, *et al.*, 2011 Package ‘lme4.’ Linear
733 mixed-effects models using S4 classes. R package version 1.

734 Baumann H., and O. Doherty, 2013 Decadal changes in the world’s coastal latitudinal temperature
735 gradients. *Plos One* 8: e67596. <https://doi.org/10.1371/journal.pone.0067596>

736 Begun D. J., and C. F. Aquadro, 1992 Levels of naturally occurring DNA polymorphism correlate with
737 recombination rates in *D. melanogaster*. *Nature* 356: 519–520. <https://doi.org/10.1038/356519a0>

738 Billerbeck J. M., T. E. Lankford, and D. O. Conover, 2001 Evolution of intrinsic growth and energy
739 acquisition rates. I. Trade-offs with swimming performance in *Menidia menidia*. *Evolution* 55:
740 1863–1872. <https://doi.org/10.1111/j.0014-3820.2001.tb00835.x>

741 Bolger A. M., M. Lohse, B. Usadel, 2014 Trimmomatic: a flexible trimmer for Illumina sequence data.
742 *Bioinformatics* 15:2114–20. <https://doi.org/10.1093/bioinformatics/btu170>

743 Branca A., T. D. Paape, P. Zhou, R. Briskine, A. D. Farmer, *et al.*, 2011 Whole-genome nucleotide
744 diversity, recombination, and linkage disequilibrium in the model legume *Medicago truncatula*.
745 *Proc National Acad Sci* 108: E864–E870. <https://doi.org/10.1073/pnas.1104032108>

746 Brandvain Y., and G. Coop, 2012 Scrambling eggs: Meiotic drive and the evolution of female
747 recombination rates. *Genetics* 190: 709–723. <https://doi.org/10.1534/genetics.111.136721>

748 Catchen J., P. A. Hohenlohe, S. Bassham, A. Amores, and W. A. Cresko, 2013 Stacks: an analysis tool
749 set for population genomics. *Mol Ecol* 22: 3124–3140. <https://doi.org/10.1111/mec.12354>

750 Charlesworth B., 1976 Recombination modification in a fluctuating environment. *Genetics* 83: 181–
751 195. <https://doi.org/10.1093/genetics/83.1.181>

752 Chovnick A., 1973 Gene conversion and transfer of genetic information within the inverted region of
753 inversion heterozygotes. *Genetics* 75: 123–131. <https://doi.org/10.1093/genetics/75.1.123>

754 Christmas M. J., A. Wallberg, I. Bunikis, A. Olsson, O. Wallerman, *et al.*, 2019 Chromosomal
755 inversions associated with environmental adaptation in honeybees. *Mol Ecol* 28: 1358–1374.
756 <https://doi.org/10.1111/mec.14944>

757 Clarke L., B. Walther, S. Munch, S. Thorrold, and D. Conover, 2009 Chemical signatures in the
758 otoliths of a coastal marine fish, *Menidia menidia*, from the northeastern United States: spatial and
759 temporal differences. *Mar Ecol Prog Ser* 384: 261–271. <https://doi.org/10.3354/meps07927>

760 Conover D. O., and B. E. Kynard, 1981 Environmental sex determination: Interaction of temperature
761 and genotype in a fish. *Science* 213: 577–579. <https://doi.org/10.1126/science.213.4507.577>

762 Conover D. O., and S. Murawski, 1982 Offshore winter migration of the Atlantic silverside, *Menidia*
763 *menidia*. Fishery bulletin United States, National Marine Fisheries Service.

764 Conover D. O., and S. W. Heins, 1987 The environmental and genetic components of sex ratio in
765 *Menidia menidia* (Pisces: Atherinidae). *Copeia* 1987: 732. <https://doi.org/10.2307/1445667>

766 Conover D. O., and T. M. C. Present, 1990 Countergradient variation in growth rate: compensation for
767 length of the growing season among Atlantic silversides from different latitudes. *Oecologia* 83:
768 316–324. <https://doi.org/10.1007/bf00317554>

769 Conover D. O., and S. B. Munch, 2002 Sustaining fisheries yields over evolutionary time scales. *Science*
770 297: 94–96. <https://doi.org/10.1126/science.1074085>

771 Conover D. O., S. A. Arnott, M. R. Walsh, and S. B. Munch, 2005 Darwinian fishery science: lessons
772 from the Atlantic silverside (*Menidia menidia*). *Can J Fish Aquat Sci* 62: 730–737.
773 <https://doi.org/10.1139/f05-069>

774 Conover D. O., T. A. Duffy, and L. A. Hice, 2009 The covariance between genetic and environmental
775 influences across ecological gradients. *Ann Ny Acad Sci* 1168: 100–129.
776 <https://doi.org/10.1111/j.1749-6632.2009.04575.x>

777 Cooney C. R., J. E. Mank, and A. E. Wright, 2021 Constraint and divergence in the evolution of male
778 and female recombination rates in fishes. *Evolution*. <https://doi.org/10.1111/evo.14357>

779 Dapper A. L., and B. A. Payseur, 2017 Connecting theory and data to understand recombination rate
780 evolution. *Philosophical Transactions Royal Soc B* 372: 20160469.
781 <https://doi.org/10.1098/rstb.2016.0469>

782 DePasquale E., H. Baumann, and C. Gobler, 2015 Vulnerability of early life stage Northwest Atlantic
783 forage fish to ocean acidification and low oxygen. *Mar Ecol Prog Ser* 523: 145–156.
784 <https://doi.org/10.3354/meps11142>

785 Dimens, P.D., 2022 pdimens/LepWrap. Zenodo Version 3.6.2. <https://doi.org/10.5281/zenodo.6055566>

786 Duffy T. A., L. A. Hice, and D. O. Conover, 2015 Pattern and scale of geographic variation in
787 environmental sex determination in the Atlantic silverside, *Menidia menidia*. *Evolution* 69: 2187–
788 2195. <https://doi.org/10.1111/evo.12724>

789 Elliott C.G., 1955 The effect of temperature on chiasma frequency. *Heredity* 9: 385–398.
790 <https://doi.org/10.1038/hdy.1955.39>

791 Faria R., P. Chaube, H. E. Morales, T. Larsson, A. R. Lemmon, *et al.*, 2019a Multiple chromosomal
792 rearrangements in a hybrid zone between *Littorina saxatilis* ecotypes. *Mol Ecol* 28: 1375–1393.
793 <https://doi.org/10.1111/mec.14972>

794 Faria R., K. Johannesson, R. K. Butlin, and A. M. Westram, 2019b Evolving Inversions. *Trends Ecol
795 Evol* 34: 239–248. <https://doi.org/10.1016/j.tree.2018.12.005>

796 Felsenstein J., 1974 The evolutionary advantage of recombination. *Genetics* 78: 737–56.

797 Georg, G. M., 2020 LambertW: An R package for Lambert W x F Random Variables. R package version
798 0.6.6.

799 Grgis H. Z., 2015 Red: an intelligent, rapid, accurate tool for detecting repeats de-novo on the genomic
800 scale. *Bmc Bioinformatics* 16: 227. <https://doi.org/10.1186/s12859-015-0654-5>

801 Haenel Q., T. G. Laurentino, M. Roesti, and D. Berner, 2018 Meta-analysis of chromosome-scale
802 crossover rate variation in eukaryotes and its significance to evolutionary genomics. *Mol Ecol* 27:
803 2477–2497. <https://doi.org/10.1111/mec.14699>

804 Hager E. R., O. S. Harringmeyer, T. B. Wooldridge, S. Theingi, J. T. Gable, *et al.*, 2021 A chromosomal
805 inversion drives evolution of multiple adaptive traits in deer mice. *bioRxiv*.
806 <https://doi.org/10.1101/2021.01.21.427490>

807 Hinch A. G., A. Tandon, N. Patterson, Y. Song, N. Rohland, *et al.*, 2011 The landscape of
808 recombination in African Americans. *Nature* 476: 170–175. <https://doi.org/10.1038/nature10336>

809 Hoffmann A. A., and L. H. Rieseberg, 2008 Revisiting the impact of inversions in evolution: From
810 population genetic markers to drivers of adaptive shifts and speciation? *Annu Rev Ecol Evol Syst*
811 39: 21–42. <https://doi.org/10.1146/annurev.ecolsys.39.110707.173532>

812 Huang S., M. Kang, and A. Xu, 2017 HaploMerger2: rebuilding both haploid sub-assemblies from high-
813 heterozygosity diploid genome assembly. *Bioinformatics* 33: btx220-.
814 <https://doi.org/10.1093/bioinformatics/btx220>

815 Jones F. C., M. G. Grabherr, Y. F. Chan, P. Russell, E. Mauceli, *et al.*, 2012 The genomic basis of
816 adaptive evolution in threespine sticklebacks. *Nature* 484: 55. <https://doi.org/10.1038/nature10944>

817 Joron M., R. Papa, M. Beltrán, N. Chamberlain, J. Mavárez, *et al.*, 2006 A conserved supergene locus
818 controls colour pattern diversity in *Heliconius* butterflies. *Plos Biol* 4: e303.
819 <https://doi.org/10.1371/journal.pbio.0040303>

820 Kim S., V. Plagnol, T. T. Hu, C. Toomajian, R. M. Clark, *et al.*, 2007 Recombination and linkage
821 disequilibrium in *Arabidopsis thaliana*. *Nat Genet* 39: 1151–1155. <https://doi.org/10.1038/ng2115>

822 Kirkpatrick M., and N. Barton, 2006 Chromosome inversions, local adaptation and speciation. *Genetics*
823 173: 419–434. <https://doi.org/10.1534/genetics.105.047985>

824 Kirkpatrick M., 2010 How and why chromosome inversions evolve. *Plos Biol* 8: e1000501.
825 <https://doi.org/10.1371/journal.pbio.1000501>

826 Kirubakaran T. G., H. Grove, M. P. Kent, S. R. Sandve, M. Baranski, *et al.*, 2016 Two adjacent
827 inversions maintain genomic differentiation between migratory and stationary ecotypes of Atlantic
828 cod. *Mol Ecol* 25: 2130–2143. <https://doi.org/10.1111/mec.13592>

829 Kong A., G. Thorleifsson, D. F. Gudbjartsson, G. Masson, A. Sigurdsson, *et al.*, 2010 Fine-scale
830 recombination rate differences between sexes, populations and individuals. *Nature* 467: 1099–1103.
831 <https://doi.org/10.1038/nature09525>

832 Korneliussen, T. S., A. Albrechtsen, & R. Nielsen, 2014 ANGSD: Analysis of Next Generation
833 Sequencing Data. *BMC Bioinformatics* 15:356. <https://doi.org/10.1186/s12859-014-0356-4>

834 Krimbas C. B., and J. R. Powell, 1992 *Drosophila inversion polymorphism*. CRC press.

835 Langmead B., and S. L. Salzberg, 2012 Fast gapped-read alignment with Bowtie 2. *Nat Methods* 9: 357–
836 359. <https://doi.org/10.1038/nmeth.1923>

837 Li H., B. Handsaker, A. Wysoker, T. Fennell, J. Ruan, *et al.*, 2009 The sequence alignment/map format
838 and SAMtools. *Bioinformatics* 25: 2078–2079. <https://doi.org/10.1093/bioinformatics/btp352>

839 Li X., C. Zhu, Z. Lin, Y. Wu, D. Zhang, *et al.*, 2011 Chromosome size in diploid eukaryotic species
840 centers on the average length with a conserved boundary. *Mol Biol Evol* 28: 1901–1911.
841 <https://doi.org/10.1093/molbev/msr011>

842 Lou R. N., N. K. Fletcher, A. P. Wilder, D. O. Conover, N. O. Therkildsen, *et al.*, 2018 Full
843 mitochondrial genome sequences reveal new insights about post-glacial expansion and regional
844 phylogeographic structure in the Atlantic silverside (*Menidia menidia*). *Mar Biol* 165: 124.
845 <https://doi.org/10.1007/s00227-018-3380-5>

846 Mansour Y., A. Chateau, and A.-S. Fiston-Lavier, 2021 BREC: an R package/Shiny app for
847 automatically identifying heterochromatin boundaries and estimating local recombination rates
848 along chromosomes. Bmc Bioinformatics 22: 396. <https://doi.org/10.1186/s12859-021-04233-1>

849 McKinney G. J., L. W. Seeb, W. A. Larson, D. Gomez-Uchida, M. T. Limborg, *et al.*, 2016 An integrated
850 linkage map reveals candidate genes underlying adaptive variation in Chinook salmon
851 (*Oncorhynchus tshawytscha*). Mol Ecol Resour 16: 769–783. <https://doi.org/10.1111/1755-0998.12479>

853 Merot C., 2020 Making the most of population genomic data to understand the importance of
854 chromosomal inversions for adaptation and speciation. Mol Ecol 29: 2513–2516.
855 <https://doi.org/10.1111/mec.15500>

856 Merot C., V. Llaurens, E. Normandeau, L. Bernatchez, and M. Wellenreuther, 2020 Balancing selection
857 via life-history trade-offs maintains an inversion polymorphism in a seaweed fly. Nat Commun 11:
858 670. <https://doi.org/10.1038/s41467-020-14479-7>

859 Muller H. J., 1964 The relation of recombination to mutational advance. Mutat Res Fundam Mol Mech
860 Mutagen 1: 2–9. [https://doi.org/10.1016/0027-5107\(64\)90047-8](https://doi.org/10.1016/0027-5107(64)90047-8)

861 Munch S. B., and D. O. Conover, 2003 Rapid growth results in increased susceptibility to predation in
862 *Menidia menidia*. Evolution 57: 2119–2127. <https://doi.org/10.1111/j.0014-3820.2003.tb00389.x>

863 Murray C. S., L. A. Fuiman, and H. Baumann, 2016 Consequences of elevated CO₂ exposure across
864 multiple life stages in a coastal forage fish. Ices J Mar Sci 74: 1051–1061.
865 <https://doi.org/10.1093/icesjms/fsw179>

866 Noor M. A. F., K. L. Grams, L. A. Bertucci, and J. Reiland, 2001 Chromosomal inversions and the
867 reproductive isolation of species. Proc National Acad Sci 98: 12084–12088.
868 <https://doi.org/10.1073/pnas.221274498>

869 Nosil P., D. J. Funk, and D. Ortiz-Barrientos, 2009 Divergent selection and heterogeneous genomic
870 divergence. Mol Ecol 18: 375–402. <https://doi.org/10.1111/j.1365-294x.2008.03946.x>

871 Otto S. P., and N. H. Barton, 1997 The evolution of recombination: removing the limits to natural
872 selection. Genetics 147: 879–906.

873 Otto S. P., and T. Lenormand, 2002 Resolving the paradox of sex and recombination. Nat Rev Genet 3:
874 252–261. <https://doi.org/10.1038/nrg761>

875 Peñalba J. V., and J. B. W. Wolf, 2020 From molecules to populations: appreciating and estimating
876 recombination rate variation. Nat Rev Genet 21: 476–492. <https://doi.org/10.1038/s41576-020-0240-1>

878 Peterson B. K., J. N. Weber, E. H. Kay, H. S. Fisher, and H. E. Hoekstra, 2012 Double digest RADseq:
879 an inexpensive method for de novo SNP discovery and genotyping in model and non-model
880 species. Plos One 7: e37135. <https://doi.org/10.1371/journal.pone.0037135>

881 Plough, H. H. 1917. The effect of temperature on crossing over in *Drosophila*. J of Exp Zool 24: 147-
882 209. <https://doi.org/10.1002/jez.1400240202>

883 Pringle J., and H. Baumann, 2019 Otolith-based growth reconstructions in young-of-year Atlantic
884 silversides *Menidia menidia* and their implications for sex-selective survival. Mar Ecol Prog Ser
885 632: 193–204. <https://doi.org/10.3354/meps13174>

886 Rastas P., 2017 Lep-MAP3: robust linkage mapping even for low-coverage whole genome sequencing
887 data. Bioinformatics 33: 3726–3732. <https://doi.org/10.1093/bioinformatics/btx494>

888 Rastas P., 2018 Lep-MAP3 SourceForge Forum. SeparateChromosomes2 parameters.

889 Rieseberg L. H., 2001 Chromosomal rearrangements and speciation. Trends Ecol Evol 16: 351–358.
890 [https://doi.org/10.1016/s0169-5347\(01\)02187-5](https://doi.org/10.1016/s0169-5347(01)02187-5)

891 Ritz K. R., M. A. F. Noor, and N. D. Singh, 2017 Variation in recombination rate: adaptive or not?
892 Trends Genet 33: 364–374. <https://doi.org/10.1016/j.tig.2017.03.003>

893 Roesti M., B. Kueng, D. Moser, and D. Berner, 2015 The genomics of ecological vicariance in
894 threespine stickleback fish. Nat Commun 6: 8767. <https://doi.org/10.1038/ncomms9767>

895 Samuk K., B. Manzano-Winkler, K. R. Ritz, and M. A. F. Noor, 2020 Natural selection shapes variation
896 in genome-wide recombination rate in *Drosophila pseudoobscura*. Curr Biol 30: 1517-1528.e6.
897 <https://doi.org/10.1016/j.cub.2020.03.053>

898 Samuk K., and M. A. F. Noor, 2021 Gene flow biases population genetic inference of recombination
899 rate. Biorxiv 2021.09.26.461846. <https://doi.org/10.1101/2021.09.26.461846>

900 Sardell J. M., and M. Kirkpatrick, 2020 Sex differences in the recombination landscape. Am Nat 195:
901 361–379. <https://doi.org/10.1086/704943>

902 Sarropoulou E., and J. M. O. Fernandes, 2011 Comparative genomics in teleost species: Knowledge
903 transfer by linking the genomes of model and non-model fish species. Comp Biochem Physiology
904 Part D Genom Proteom 6: 92–102. <https://doi.org/10.1016/j.cbd.2010.09.003>

905 Schultz E. T., D. O. Conover, and A. Ehtisham, 1998 The dead of winter: size-dependent variation and
906 genetic differences in seasonal mortality among Atlantic silverside (Atherinidae: *Menidia menidia*)
907 from different latitudes. Can J Fish Aquat Sci 55: 1149–1157. <https://doi.org/10.1139/f97-320>

908 Schwarzkopf E. J., J. C. Motamayor, and O. E. Cornejo, 2020 Genetic differentiation and intrinsic
909 genomic features explain variation in recombination hotspots among cocoa tree populations. Bmc
910 Genomics 21: 332. <https://doi.org/10.1186/s12864-020-6746-2>

911 Singer A., H. Perlman, Y. Yan, C. Walker, G. Corley-Smith, *et al.*, 2002 Sex-specific recombination
912 rates in zebrafish (*Danio rerio*). Genetics 160: 649–657. <https://doi.org/10.1093/genetics/160.2.649>

913 Smith J. M., 1978 *The evolution of sex*. Cambridge University Press.

914 Smukowski C. S., and M. A. F. Noor, 2011 Recombination rate variation in closely related species.
915 Heredity 107: 496–508. <https://doi.org/10.1038/hdy.2011.44>

916 Sodeland M., P. E. Jorde, S. Lien, S. Jentoft, P. R. Berg, *et al.*, 2016 “Islands of divergence” in the
917 Atlantic cod genome represent polymorphic chromosomal rearrangements. Genome Biol Evol 8:
918 1012–1022. <https://doi.org/10.1093/gbe/evw057>

919 Stapley J., P. G. D. Feulner, S. E. Johnston, A. W. Santure, and C. M. Smadja, 2017 Variation in
920 recombination frequency and distribution across eukaryotes: patterns and processes. Philosophical
921 Transactions Royal Soc B Biological Sci 372: 20160455. <https://doi.org/10.1098/rstb.2016.0455>

922 Stefansson H., A. Helgason, G. Thorleifsson, V. Steinhorsdottir, G. Masson, *et al.*, 2005 A common
923 inversion under selection in Europeans. Nat Genet 37: 129–137. <https://doi.org/10.1038/ng1508>

924 Stevison L. S., S. Sefick, C. Rushton, and R. M. Graze, 2017 Recombination rate plasticity: revealing
925 mechanisms by design. Philosophical Transactions Royal Soc B Biological Sci 372: 20160459.
926 <https://doi.org/10.1098/rstb.2016.0459>

927 Sturtevant A. H., and G. W. Beadle, 1936 The relations of inversions in the X chromosome of
928 *Drosophila melanogaster* to crossing over and disjunction. Genetics 21: 554–604.

929 Tang, H., X. Zhang, C. Miao, J. Zhang, R. Ming, J. C. Schnable, *et al.*, 2015 ALLMAPS: robust scaffold
930 ordering based on multiple maps. Genome Biol, 16:1-15. <https://doi.org/10.1186/s13059-014-0573-1>

931 Team R. C., 2020 R: 2019. A Language and Environment for Statistical Computing version 3.

932 Therkildsen N. O., A. P. Wilder, D. O. Conover, S. B. Munch, H. Baumann, *et al.*, 2019 Contrasting
933 genomic shifts underlie parallel phenotypic evolution in response to fishing. Science 365: 487–490.
934 <https://doi.org/10.1126/science.aaw7271>

935 Therkildsen N. O., and H. Baumann, 2020 A comprehensive non-redundant reference transcriptome
936 for the Atlantic silverside *Menidia menidia*. Mar Genom 53: 100738.
937 <https://doi.org/10.1016/j.margen.2019.100738>

938 Thompson M. J., and C. D. Jiggins, 2014 Supergenes and their role in evolution. Heredity 113: 1–8.
939 <https://doi.org/10.1038/hdy.2014.20>

940 Tigano A., and V. L. Friesen, 2016 Genomics of local adaptation with gene flow. Mol Ecol 25: 2144–
941 2164. <https://doi.org/10.1111/mec.13606>

942 Tigano A., A. Jacobs, A. P. Wilder, A. Nand, Y. Zhan, *et al.*, 2021a Chromosome-level assembly of the
943 Atlantic silverside genome reveals extreme levels of sequence diversity and structural genetic
944 variation. Genome Biol Evol 13: evab098. <https://doi.org/10.1093/gbe/evab098>

945 Tigano A., R. Khan, A. D. Omer, D. Weisz, O. Dudchenko, *et al.*, 2021b Chromosome size affects
946 sequence divergence between species through the interplay of recombination and selection.
947 Biorxiv 2021.01.15.426870. <https://doi.org/10.1101/2021.01.15.426870>

948 Todesco M., G. L. Owens, N. Bercovich, J.-S. Léga  , S. Soudi, *et al.*, 2020 Massive haplotypes underlie
949 ecotypic differentiation in sunflowers. *Nature* 584: 602–607. [https://doi.org/10.1038/s41586-020-
2467-6](https://doi.org/10.1038/s41586-020-
950 2467-6)

951 Villoutreix, R., D. Ayala, M. Joron, Z. Gompert, J. L. Feder, and P. Nosil, 2021 Inversion breakpoints
952 and the evolution of supergenes. *Mol Eco*, 30(12), 2738-2755. <https://doi.org/10.1111/mec.15907>

953 Warkentine B. E., C. L. Smith, and J. W. Rachlin, 1987 A reevaluation of the karyotype of the Atlantic
954 silverside, *Menidia menidia*. *Copeia* 1987: 222. <https://doi.org/10.2307/1446059>

955 Wellenreuther M., and L. Bernatchez, 2018 Eco-evolutionary genomics of chromosomal inversions.
956 *Trends Ecol Evol*. <https://doi.org/10.1016/j.tree.2018.04.002>

957 Wellenreuther M., C. M  rot, E. Berdan, and L. Bernatchez, 2019 Going beyond SNPs: The role of
958 structural genomic variants in adaptive evolution and species diversification. *Mol Ecol* 28: 1203–
959 1209. <https://doi.org/10.1111/mec.15066>

960 Wilder A. P., S. R. Palumbi, D. O. Conover, and N. O. Therkildsen, 2020 Footprints of local adaptation
961 span hundreds of linked genes in the Atlantic silverside genome. *Evol Lett* 4: 430–443.
962 <https://doi.org/10.1002/evl3.189>

963 Wu J., H. Mizuno, M. Hayashi-Tsugane, Y. Ito, Y. Chiden, *et al.*, 2003 Physical maps and
964 recombination frequency of six rice chromosomes. *Plant J* 36: 720–730.
965 <https://doi.org/10.1046/j.1365-313x.2003.01903.x>

966 Yeaman S., 2013 Genomic rearrangements and the evolution of clusters of locally adaptive loci. *Proc
967 National Acad Sci* 110: E1743–E1751. <https://doi.org/10.1073/pnas.1219381110>